Evaluation of an Integrin $a_v\beta_3$ and Aminopeptidase N Dual-Receptor Targeting Tracer for Breast Cancer Imaging

Yongkang Gai[†,‡,∥], **Yaqun Jiang**[†,‡,∥], **Yu Long**[†,‡], **Lingi Sun**[§], **Qingyao Liu**[†,‡], **Chunxia Qin**[†,‡], **Yongxue Zhang**[†,‡], **Dexing Zeng**[*,§], **Xiaoli Lan**[*,†,‡]

[†]Department of Nuclear Medicine, Union Hospital, Tongji Medical College, Huazhong University of Science and Technology, Wuhan 430022, China

[‡]Hubei Province Key Laboratory of Molecular Imaging, Wuhan 430022, China

[§]Center for Radiochemistry Research, Department of Diagnostic Radiology, Oregon Health & Science University, Portland, Oregon 97239, United States

Abstract

Integrin $a_v\beta_3$ and aminopeptidase N (APN, also known as CD13) are two important targets involved in the regulation of angiogenesis, tumor proliferation, invasion, and metastasis. In this study, we developed a heterodimeric tracer consisting of arginine–glycine-aspartic (RGD) and asparagine–glycine-arginine (NGR) peptides targeting $a_v\beta_3$ and CD13, respectively, for PET imaging of breast cancer. The NGR peptide was first modified with N_3-NO^tB_2 and then conjugated to BCN-PEG$_4$-c(RGDyK) via copper-free click chemistry. The resulting precursor was purified and radiolabeled with gallium-68. Small-animal PET/CT imaging and post-imaging biodistribution studies were performed in mice bearing human breast cancer MCF-7, MDA-MB-231, MDA-MB-468, and MX-1 xenografts and pulmonary metastases models. The expression levels of $a_v\beta_3$ and CD13 in tumors were checked via immunochemical staining. The heterodimeric tracer was successfully synthesized and radiolabeled with gallium-68 at a molar activity of 45–100 MBq/nmol at the end of synthesis. It demonstrated high in vitro and in vivo stability. In static PET/CT imaging studies, the MCF-7 tumor could be clearly visualized and exhibited higher uptake at 30 min post injection of ^{68}Ga-NGR-RGD than that of either ^{68}Ga-RGD or ^{68}Ga-NGR alone. High specificity was shown in blocking studies using Arg-Gly-Asp (RGD) and Asp-Gly-Arg (NGR) peptides. The MCF-7 tumor exhibited the highest uptake of ^{68}Ga-NGR-RGD followed by MDA-MB-231, MDA-MB-468, and MX-1 tumors. This was consistent with their expression levels of CD13 and $a_v\beta_3$ as confirmed by western blot and immunohistochemical staining. Metastatic lesions in the lungs were clearly detectable on ^{68}Ga-NGR-RGD PET/CT imaging in mouse models of pulmonary metastases. ^{68}Ga-NGR-RGD, a CD13 and $a_v\beta_3$ dual-receptor targeting tracer, showed higher binding avidities, targeting efficiency, and longer tumor

[*]**Corresponding Authors**: zengd@ohsu.edu. Phone: 503-494-5946. Fax: 503494-4749 (D.Z.).; LXL730724@hotmail.com. Phone: +86-2783692633. Fax: +86-27-85726282 (X.L.).
[∥]Author Contributions
Y.G. and Y.J. contributed equally to this work.

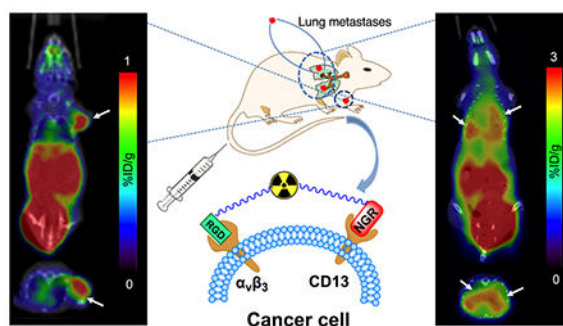retention time compared with ^{68}Ga-NGR and ^{68}Ga-RGD. Its promising in vivo performance makes it an ideal candidate for future clinical Monomeric translation.

Graphical Abstract

Keywords

breast cancer; angiogenesis; CD13; integrin $\alpha_v\beta_3$; dual-receptor targeted

1. INTRODUCTION

Angiogenesis is an important demand to provide oxygen and nutrients for tumor growth, progression, invasion, and metastasis,[1,2] making its targeting one of the most attractive approaches to the diagnosis and therapy of malignancies.[3] Modulation of angiogenesis relies on migration and invasion of vascular endothelial cells, which are mainly regulated by vascular endothelial growth factor receptors (VEGFRs), matrix metalloproteases (MMPs), and cell adhesion receptor integrins.[4] Biological markers, such as aminopeptidase N (APN/CD13) and integrins, especially integrin $\alpha_v\beta_3$, are selectively overexpressed in the endothelial cells of proliferating vessels and tumor cells, participating in the progression of malignancy, including enhancing the invasiveness of tumor cells, proliferation, and angiogenesis.[5–8] Given these characteristics, they are widely studied as efficient cell surface targets for cancer diagnosis and anticancer therapy.

RGD (Arg-Gly-Asp) and NGR (Asp-Gly-Arg) motifs have been recognized as well-known peptide sequences for targeting integrin $\alpha_v\beta_3$ and CD13, respectively.[9] Although a series of monoreceptor-targeted tracers based on RGD or NGR have exhibited good in vivo performance for tumor imaging, these monoreceptor tracers suffer several drawbacks including relatively low binding affinity, short tumor retention time, and low tumor uptake.[10] Since many tumors overexpress multiple receptors, probes that can recognize multiple targets could acquire higher targeting affinity and efficiency than those of their monoreceptor peers. Therefore, a multivalent interaction strategy, which can convert low-affinity ligands to high-avidity ones and increases the maximum binding capacity, is a promising strategy to overcome these drawbacks.[10,11]

Breast cancer is the most common type of malignancy diagnosed in women with high incidence and mortality rates.[12] Among all women diagnosed with breast cancer,

approximately 50% of them develop metastases.[13] Over 90% of breast cancer-related deaths are attributed to metastasis and metastasis-related complications.[14] The commonest sites of metastatic spread are the lungs, bone, liver, and brain. In particular, lung metastases tend to occur within five years of initial diagnosis of breast cancer.[15] Therefore, diagnosis and metastasis detection are essential for management of breast cancer. In breast cancer, the expression levels of $\alpha_v\beta_3$ and CD13 in serum and tumor tissue were correlated with tumor type, neoangiogenesis, invasiveness, metastasis, and overall survival, serving as poor prognostic factors.[16,17] Other than diagnosis, the ligands RGD and NGR of $\alpha_v\beta_3$ and CD13 also could be applied for cancer therapy, such as anti-angiogenesis drugs and radionuclide therapy.[1,2,7,18] Therefore, measuring these expression levels may help monitor cancer progression and help in the tailoring of treatment plans.

The purpose of this study was to develop a radiolabeled heterodimeric tracer targeting both CD13 and integrin $\alpha_v\beta_3$ and evaluate the feasibility and preclinical diagnosis value of the resulting probe (^{68}Ga-NGR-RGD) in breast cancer xenograft mice, compared with ^{68}Ga-labeled monomeric NGR and RGD tracers. In addition, the utility of ^{68}Ga-NGR-RGD in detecting metastatic lesions was also investigated using breast cancer lung metastasis mouse models.

2. MATERIALS AND METHODS

2.1. Reagents and Instruments.

[^{68}Ga]GaCl$_3$ was produced with a ^{68}Ge/^{68}Ga generator (Isotope Technologies Garching GmbH, Garching, Germany). Peptides were purchased from Chinapeptide (Shanghai, China) or Gl Biochem (Shanghai, China). Endo-BCN-PEG$_4$-NHS ester was purchased from Broadpharm (San Diego CA, U.S.A.). 2,2′,2″-(2-(4-isothiocyanatobenzyl)-1,4,7-triazonane-1,4,7-triyl)triacetic acid (p-SCN-Bn-NOTA) was purchased from Macrocyclics (Dallas TX, U.S.A.). NOTA-Bn-thioureidocyclic(Arg-Gly-Asp-D-Tyr-Lys) (NOTA-c(RGDyK)) and NOTA-Bn-thioureido-cyclic(Lys-Asn-Gly-Arg-Glu) (NOTA-c(KNGRE)) were synthesized according to published methods.[19,20] All other chemicals were purchased from J&K Chemicals (Beijing, China), Adamas Reagent Co., Ltd., (Shanghai, China), or Sigma-Aldrich (St. Louis MO, U.S.A.), unless indicated otherwise. The chemicals were used directly without further purification. Radioactivity of all samples was quantified by an automatic γ counter (2470 WIZARD; PerkinElmer, Waltham MA, U.S.A.). TransPET Discoverist 180 small-animal PET/CT (Raycan Technology Co., Ltd., Suzhou, China) and lnliView-3000B small-animal PET/SPECT/CT (Novel Medical, Beijing, China) were used to visualize mice with xenografted tumors. High-performance liquid chromatography (HPLC) was performed on LC-20AT (Shimadzu Corporation, Tokyo, Japan) equipped with a SPD-20A UV–vis detector and a flow count radiation detector (Bioscan, Washington DC, U.S.A.). The radiochemical yield and radiochemical purity of the tracers were determined by HPLC using a 4.6 × 250 mm Luna C$_{18}$ column (Phenomenex, CA, U.S.A.). The column was eluted at a flow rate of 1 mL/min at 25 °C with a gradient of 5%-90% MeCN/H$_2$O with 0.1% trifluoroacetic acid (TFA) in 10 min.

2.2. Synthesis of NGR-RGD.

NGR-RGD was synthesized using our previously developed method.[21] Briefly, the bifunctional chelator $NO2A_{tBu}$-N_3 was conjugated to the peptide NH_2-PEG_4-c(RGDyK), and N_3-NOTA-PEG_4-c(RGDyK) was obtained after TFA deprotection and HPLC purification. The cyclic peptide c(CNGRC) was modified with endo-BCN-PEG_4-NHS ester to obtain BCN-PEG_4-c(CNGRC). The heterodimeric tracer c(RGDyK)-PEG_4-NOTA-click-PEG_4-c(CNGRC) (NGR-RGD) was obtained via copper-free click chemistry by mixing them at a molar ratio of 1:1 (Scheme S1). High-resolution mass spectrometry (HRMS) (Bruker SolariX 7.0 T, Bruker Daltonik, Bremen, Germany): m/z calcd for $C_{94}H_{151}N_{27}O_{33}S_2$ $[M + 2H]^{2+}$, 1126.0283; found, 1126.0427.

2.3. Radiolabeling.

In brief, 2 μL of NGR-RGD, NOTA-c(RGDyK), or NOTA-c(KNGRE) (2 mM) was added to 150 μL of buffer (0.25 M sodium acetate, pH 6.8). Subsequently, 500 μL of $[^{68}Ga]GaCl_3$ in 0.05 M HCl (180–400 MBq) was added and mixed. The final pH of the reaction mixture was approximately 4.0. Then, the reaction mixture was heated to 90 °C and reacted for 5 min. After cooling to room temperature, ^{68}Ga-NGR-RGD, ^{68}Ga-NOTA-c(RGDyK) (denoted as ^{68}Ga-RGD), and ^{68}Ga-NOTA-c(KNGRE) (denoted as ^{68}Ga-NGR) were obtained and used for the subsequent studies without further purification. The reaction mixture (1 μL) was subjected to HPLC for analysis using the method described above.

2.4. Stability and Partition Coefficient.

^{68}Ga-NGR-RGD (14.8 MBq) was incubated in phosphate buffer saline (PBS, pH 7.4) as well as fresh human serum at 37 °C for 2 h. For the serum sample, an equal volume of acetonitrile was added to the sample, and the sample was centrifuged at a speed of 13,000g for 5 min for the purpose of precipitating plasma proteins. The supernatant was then subjected to analysis. The radiochemical purities of the tracer samples were evaluated by analytical HPLC under the conditions described above.

Normal BALB/c nude mice were used to evaluate the in vivo stability of ^{68}Ga-NGR-RGD. Mice were anesthetized intraperitoneally with 1% sodium pentobarbital aqueous solution (0.1 mL/20 g mouse). Each mouse was injected via the tail vein with ^{68}Ga-NGR-RGD (74 MBq). A urine sample was collected at 2 h post injection (p.i.), treated with acetonitrile, and centrifuged to remove proteins. The supernatant was analyzed by radio-HPLC.

PBS (1.0 mL, pH 7.4) and 1-octanol (1.0 mL) were mixed. Then, 5 μL of ^{68}Ga-NGR-RGD (740 kBq), ^{68}Ga-RGD (740 kBq), or ^{68}Ga-NGR (740 kBq) was respectively added to the mixed solution. The mixture was then continuously vortexed for 5 min and centrifuged (4000 rpm, 5 min). Samples (100 μL) of each phase were measured by a γ counter. The partition coefficient was calculated as follows: log $P = \log_{10}$(counts in 1-octanol/counts in PBS).

2.5. Cell Culture.

Human breast cancer cells, MCF-7, MDA-MB-231, and MDA-MB-468, were derived from our own laboratory preservation. MX-1 was donated by Basic Medical College of Huazhong

University of Science and Technology. MCF-7 and MX-1 cells were cultivated in Dulbecco's modified Eagle high-glucose medium (DMEM; Gibco, Carlsbad CA, U.S.A.) with 10% fetal bovine serum (Sciencell, Carlsbad CA, U.S.A.), 100 mg/mL streptomycin, and 100 mg/mL penicillin (Solarbio, Shanghai, China) at 37 °C in a humidified incubator containing 5% CO_2. MDA-MB-231 and MDA-MB-468 were cultivated in Leibovitz's L-15 medium without CO_2 equilibration.

2.6. Western Blot Analysis.

MCF-7, MDA-MB-231, MDA-MB-468, and MX-1 cells were lysed with a RIPA lysis buffer (Beyotime, Haimen, China), and the protein concentration was determined using a BCA protein assay kit (Aidlab, Beijing, China). Afterward, the target protein was denatured and separated by SDS-PAGE and transferred to a poly-vinylidene fluoride (PVDF) membrane. The blots were incubated with specific primary antibodies (anti-CD13, anti-integrin α_v, and anti-integrin β_3, diluted 1:1000; Abcam, Cambridge MA, U.S.A.) followed by goat anti-rabbit IgG/HRP (diluted 1:20000; Sungene, Tianjin, China). Glyceraldehyde-3-phosphate dehydrogenase (GAPDH) was used as the internal control. The membranes were detected by enhanced chemiluminescence (ECL kit, Beyotime) and analyzed using Quantity One software (Bio-Rad, Hercules CA, U.S.A.).

2.7. In Vitro Cell Uptake and Blocking Studies.

MCF-7, MDA-MB-231, MDA-MB-468, and MX-1 cells were cultivated to 80–90% confluence and then were counted using a cytometer (Cellometer Mini, Nexcelom Bioscience LLC, Lawrence MA, U.S.A.). Cells were seeded into 24-well plates (2×10^5 cells per well, three duplicate wells in each group) one day in advance. In order to compare the cell uptake among the three tracers, MCF-7 was used for cell uptake measurements of ^{68}Ga-NGR-RGD, ^{68}Ga-RGD, and ^{68}Ga-NGR. Probes of 50 μL (1 pmol, 74 kBq) were added to each well and incubated at 37 °C for 30 min, 1 h, and 2 h. When each time point was reached, the supernatant of each well was removed and placed in a tube; each well was washed three times with pre-cooled PBS and placed in the same tube of the supernatant. The cells were then lysed by 1 N sodium hydroxide. Afterward, the cell lysate was placed into another tube, and each well was washed three times with pre-cooled PBS and placed in the same tube. The radioactivity of each tube was measured with a γ counter.

A blocking study was conducted in MCF-7 cells. One group of cells was only incubated with ^{68}Ga-NGR-RGD (50 μL, 74 KBq) for 2 h at 37 °C. The other groups were pretreated with 100 times excess of nonradioactive RGD, NGR, RGD+NGR, or NGR-RGD (100 pmol) 15 min in advance and then incubated with ^{68}Ga-NGR-RGD (50 μL, 74 kBq) for 2 h at 37 °C. For evaluation of the uptake of ^{68}Ga-NGR-RGD by different tumor types, MCF-7, MDA-MB-231, MDA-MB-468, and MX-1 cells were used.

2.8. Animal Models.

All animal studies were conducted according to the guidelines of the Institutional Animal Care and Use Committee of Tongji Medical College of Huazhong University of Science and Technology. Female BALB/c nude mice (4–5 weeks old and 7 weeks old) were purchased from Beijing HFK Bioscience Co. Ltd. (Beijing, China) and raised in a specific pathogen-

free barrier system room. For xenograft tumor models, BALB/c nude mice were subcutaneously injected in the right shoulder with a cell suspension of 1.0×10^7 (125 μL) MCF-7, MDA-MB-231, MDA-MB-468, or MX-1. The mice were subjected to the following experiments when tumor sizes reached 0.8–1.0 cm.

The breast cancer lung metastasis model was developed according to published procedures.[22,23] In brief, MCF-7 cells were harvested and resuspended in a mixed solution of matrigel and PBS. Female BALB/c nude mice were anesthetized intraperitoneally with 1% sodium pentobarbital aqueous solution (0.1 mL/20 g) and placed in a right lateral decubitus position. A 0.5 cm longitudinal incision was made at the lower edge of the scapula, and the muscle layer was bluntly separated to expose the ribs. Then, 20 μL cell suspensions of approximately 3×10^6 MCF-7 cells were injected directly into the left lobe of the lung through the intercostal space. Skin incisions were closed, and the mice were kept warm until fully alert. One month later, the mice underwent PET/CT imaging.

2.9. Animal PET/CT Imaging.

For the purpose of comparison of different tracers, each group of MCF-7 tumor xenograft mice were administered ^{68}Ga-NGR-RGD, ^{68}Ga-RGD, and ^{68}Ga-NGR (6.5–9 MBq, 125 μL) via the tail vein ($n = 4$ each group). The mice were anesthetized and maintained with 2.0% isoflurane in 100% oxygen. They were placed on an examining table in the prone position and underwent PET/CT imaging at 30 min p.i. To assess the specificity of ^{68}Ga-NGR-RGD, blocking experiments were performed in MCF-7 tumor models. The blocking agents RGD, NGR, RGD+NGR, and NGR-RGD (20 mg/kg, approximately 500 μg/mouse) were coinjected with ^{68}Ga-NGR-RGD (6.5–9 MBq, 125 μL). The MCF-7, MDA-MB-231, MDA-MB-468, and MX-1 tumor xenograft mice were injected via the tail vein (n = 4 each group) with ^{68}Ga-NGR-RGD (6.5–9 MBq, 125 μL) and underwent a PET/CT scan at 30 min p.i.

The breast cancer lung metastasis model mice underwent a PET/CT scan at 1 h p.i. of ^{68}Ga-NGR-RGD (6.5–9 MBq, 125 μL, $n = 3$).

2.10 Biodistribution Studies.

After PET/CT scanning, all the mice were euthanized at 1 h time point, and the tissues of interest were collected, weighed, and counted using an automatic γ counter. The radioactivity of each organ and tissue was expressed as the percentage of the injected dose per gram of tissue (%ID/g) and corrected for radioactive decay.

2.11. Immunohistochemistry Analysis.

After PET/CT imaging, the tumor tissues were collected, fixed in 4% paraformaldehyde, and then dehydrated and embedded in paraffin. The tumor sections (5 μm) were dewaxed and rehydrated. The sections were rinsed with EDTA buffer (pH 9.0) and blocked with 3% hydrogen peroxide and 10% normal goat serum. The sections were incubated with primary antibodies (anti-CD13, anti-$\alpha_v\beta_3$, and anti-CD3; 1:100; Abcam, Cambridge MA, U.S.A.) at 4 °C overnight. Then, the tissue slices were incubated with a secondary antibody (HRP-labeled goat anti-rabbit IgG, diluted 1:50, Abbkine, Redlands CA, U.S.A.) at room temperature for 25 min. The sections were stained with 3,3′-diaminobenzidine (DAB,

Beyotime, Hangzhou, China) for 5 min followed by counter-staining with hematoxylin (Beyotime) for 1 min and were observed under light microscopy.

2.12. Statistical Analysis.

Data are expressed as mean ± SD. Statistical analysis was performed using one-way ANOVA or Studen's t-test with commercial software (GraphPad Prism 8, GraphPad, Inc., San Diego CA, USA). $P < 0.05$ indicates statistical significance.

3. RESULTS

3.1. Chemical and Radiochemical Characterization.

The heterodimeric tracer NGR-RGD was characterized by HRMS and analytical HPLC. The labeling procedures for ^{68}Ga-NGR-RGD, ^{68}Ga-RGD, and ^{68}Ga-NGR were straightforward with high radiochemical yields (>99%), and all radiolabeled tracers were used directly without further purification. The molar activity was 45–100 MBq/nmol at the end of synthesis. The in vitro and in vivo stability of ^{68}Ga-NGR-RGD was tested. As shown in Figure 1, the proportion of the intact tracer exceeded 95% after incubation in PBS and serum at 37 °C for 2 h, indicating that the tracer was stable and suitable for the subsequent in vitro and in vivo experiments. Since ^{68}Ga-NGR-RGD is mainly excreted by the kidney-urine pathway, urine samples were collected at 2 h post injection to determine its in vivo stability. No obvious disassociated ^{68}Ga was observed in the urine samples (Figure 1), indicating a good in vivo stability. The log P values of ^{68}Ga-NGR-RGD, ^{68}Ga-NGR, and ^{68}Ga-RGD were -3.58 ± 0.29, -2.82 ± 0.02, and -3.22 ± 0.02, respectively, showing their high hydrophilic nature.

3.2. Characterization of Target Protein Expression in Cells.

Western blot assay was performed to characterize the expression of target proteins in the four types of breast cancer cells. As shown in Figure 2, a high CD13 expression level was observed in MCF-7 cells, while MDA-MB-468 cells showed lower expression. No obvious CD13 expression was found in either MDA-MB-231 or MX-1 cells. MDA-MB-231 cells showed the highest expression level of integrin α_v as well as integrin β_3 among the four cell lines followed by MDA-MB-468 cells and MCF-7 cells. Expression of neither integrin α_v nor integrin β_3 was observed in MX-1 cells. Therefore, MCF-7 was expected to have the highest response toward the heterodimer as it overexpressed CD13, integrin α_v, and integrin β_3.

3.3. In Vitro Cell Study.

As illustrated in Figure 3A, the uptake of ^{68}Ga-NGR-RGD by MCF-7 cells increased gradually over time and reached a maximum at 2 h, which was significantly higher than that of ^{68}Ga-NGR ($P < 0.001$) and ^{68}Ga-RGD ($P < 0.001$). Cell blocking studies were conducted to evaluate the specificity of ^{68}Ga-NGR-RGD in vitro (Figure 3B). The uptake of ^{68}Ga-NGR-RGD by MCF-7 cells decreased significantly when pretreated with excess of blocking agents RGD ($P < 0.01$), NGR ($P < 0.05$), RGD+NGR ($P < 0.05$), and NGR-RGD ($P < 0.001$). The uptake of ^{68}Ga-NGR-RGD by MCF-7 cells was higher than that of MDA-MB-231 ($P < 0.01$), MDA-MB-468 ($P < 0.001$), and MX-1 ($P < 0.001$) (Figure 3C).

3.4. Small-Animal PET/CT Imaging.

PET/CT scans were conducted to investigate the in vivo tumor targeting efficiency of the tracers. Small-animal PET/CT scans were carried out 30 min p.i. of the heterodimeric tracer ^{68}Ga-NGR-RGD or either of monomeric ^{68}Ga-RGD or ^{68}Ga-NGR into MCF-7 xenograft mice. As shown in Figure 4A, ^{68}Ga-NGR-RGD, ^{68}Ga-RGD, and ^{68}Ga-NGR mainly accumulated in kidneys and bladder, indicating renal excretion. MCF-7 tumors could be clearly visualized at 30 min p.i. of ^{68}Ga-NGR-RGD and ^{68}Ga-RGD, whereas the tumor uptake of ^{68}Ga-NGR was much lower, demonstrating the decent tumor targeting efficiency of ^{68}Ga-NGR-RGD and ^{68}Ga-RGD.

To evaluate the in vivo specific uptake of ^{68}Ga-NGR-RGD, blocking studies were conducted in MCF-7 xenograft mice. Uptakes of all MCF-7 tumors were decreased when coinjected with blocking doses of nonradioactive RGD, RGD+NGR, and NGR-RGD (Figure 4C). In the NGR peptide-blocking group, the MCF-7 tumor was partially blocked but still visible, which might be due to the rapid metabolism of the NGR peptide and the strong affinity of the RGD counterpart. The region of interest (ROI) was drawn to quantify the uptake of tumors in all groups (Figure 4B). The uptake of ^{68}Ga-NGR-RGD (1.06 ± 0.05 %ID/g) in MCF-7 was higher than that of ^{68}Ga-RGD (0.85 ± 0.10 %ID/g, $P < 0.05$) and ^{68}Ga-NGR (0.21 ± 0.09 % ID/g, $P < 0.001$). The uptake of ^{68}Ga-NGR-RGD in MCF-7 could be blocked by excess of unlabeled RGD (0.37 ± 0.05 % ID/g, $P < 0.001$), NGR (0.80 ± 0.03 %ID/g, $P < 0.001$), RGD +NGR (0.31 ± 0.03 %ID/g, $P < 0.001$), and NGR-RGD (0.28 ± 0.06 %ID/g, $P < 0.001$).

To further evaluate the utility of ^{68}Ga-NGR-RGD in breast cancer, small-animal PET/CT scans were also performed in mice bearing MDA-MB-231, MDA-MB-468, and MX-1 xenografts (Figure 5A). MDA-MB-231 tumors could be clearly visualized by ^{68}Ga-NGR-RGD with intensity comparable to that of MCF-7 tumors, whereas the intensity of MDA-MB-468 tumors was much fainter. No obvious accumulation was observed in MX-1 tumors. The overall PET imaging results were consistent with the previous western blot studies, indicating the superior specificity of the developed heterodimeric tracer. The region of interest (ROI) was drawn to quantify the uptake of MCF-7, MDA-MB-231, MDA-MB-468, and MX-1 tumors (Figure 5B). The uptake of ^{68}Ga-NGR-RGD in MCF-7 (1.03 ± 0.08 %ID/g) was comparable to MDA-MB-231 (1.04 ± 0.06 %ID/g, $P > 0.05$) and higher than that of MDA-MB-468 (0.76 ± 0.10 %ID/g, $P < 0.01$) and MX-1 (0.41 ± 0.08 %ID/g, $P < 0.001$).

To investigate the potential application of ^{68}Ga-NGR-RGD in detecting metastatic lesions, MCF-7 xenograft models in the lung were established to simulate lung metastasis from breast cancer. The longest diameter of the lung metastases was 2–5 mm (3 mice, more than 10 metastases). As shown in Figure 6A, high radioactivity accumulation was observed in the left lungs of all three mice. There was also a high uptake in the right lung of mouse 2, which were believed to be diffuse metastatic lesions (Figure 6B). The hematoxylin–eosin (HE) staining confirmed that these lesions were tumor tissues (Figure 6C).

3.5. Biodistribution Studies.

Post-imaging biodistribution studies were conducted at 1 h p.i. of ^{68}Ga-NGR-RGD, ^{68}Ga-RGD, or ^{68}Ga-NGR. As shown in Figure 7A, all three tracers showed the highest accumulations in the kidneys (2.52 ± 0.30, 1.05 ± 0.24, and 0.87 ± 0.04 %ID/g), indicating that renal clearance is the major metabolic pathway, which is consistent with the imaging results. In MCF-7 xenograft mice, the tumor uptake of ^{68}Ga-NGR-RGD (1.02 ± 0.16 %ID/g) was significantly higher than that of ^{68}Ga-RGD (0.76 ± 0.20 % ID/g, $P < 0.05$) and ^{68}Ga-NGR (0.14 ± 0.04 %ID/g, $P < 0.001$) (Figure 7C). Furthermore, the uptake of ^{68}Ga-NGR-RGD in all organs of interest was higher than that of ^{68}Ga-RGD or ^{68}Ga-NGR Tumor uptakes were significantly reduced when blocked with RGD (0.17 ± 0.04 %ID/g, $P < 0.001$), NGR (0.67 ± 0.02 %ID/g, $P < 0.05$), RGD+NGR (0.20 ± 0.07 %ID/g, $P < 0.001$), and NGR-RGD (0.16 ± 0.04 %ID/g, $P < 0.001$), (Figure 7D).

The biodistribution results of ^{68}Ga-NGR-RGD in mice bearing different kinds of breast cancer xenografts are shown in Figure 7B,E. The average tumor uptake of MCF-7 xenograft mice (1.02 ± 0.16%ID/g) was significantly higher than that of MDA-MB-231 (0.53 ± 0.05%ID/g, $P < 0.01$), MDA-MB-468 (0.28 ± 0.04%ID/g, $P < 0.001$), and MX-1 (0.20 ± 0.03%ID/g, $P < 0.001$), demonstrating the excellent ability to target tumors expressing both CD13 and integrin $a_v\beta_3$.

3.6. Immunohistochemistry Staining in Tumor Tissues.

To further validate the in vivo expression levels of CD13 and integrin $a_v\beta_3$, the tumor tissues were collected and immunohistochemistry was performed. As shown in Figure 5C, high CD13 expression levels were observed in MCF-7 tissue followed by MDA-MB-468. No obvious CD13 expression was found in either MDA-MB-231 or MX-1 tissues. The MDA-MB-231 tumor showed the highest expression level of $a_v\beta_3$ among the four tumor tissues, while MCF-7 and MDA-MB-468 tumor tissues showed lower expression of integrin $a_v\beta_3$. No obvious integrin $a_v\beta_3$ expression was observed in MX-1. The cell junction protein cluster of differentiation 31 (CD31) staining was also performed to evaluate the vascularization of the tumors. All tumor tissues exhibited neovascularity with the MDA-MB-231 tumor showing the highest density of blood vessels followed by the MCF-7 tumor. The results of tumor tissue immunohistochemistry corresponded with those of the cellular western blot.

4. DISCUSSION

In this study, a heterodimeric tracer was successfully synthesized and radiolabeled with ^{68}Ga with high radiochemical yield and purity. To the best of our knowledge, this is the first investigation for the application of conjugating RGD and NGR as a heterodimeric probe for breast cancer imaging. The radiolabeling procedure was straightforward, and the resulting tracer ^{68}Ga-NGR-RGD is stable in PBS and serum for up to 2 h. In vitro cell studies showed that higher uptake of ^{68}Ga-NGR-RGD compared with its monomeric counterparts ^{68}Ga-NGR and ^{68}Ga-RGD demonstrated superior targeting affinity and efficiency of ^{68}Ga-NGR-RGD. Cell blocking studies further validated the specific binding of ^{68}Ga-NGR-RGD to both integrin $a_v\beta_3$ and CD13 receptors.

In vivo PET/CT imaging and biodistribution studies showed that MCF-7 tumors could be distinctly visualized by either ^{68}Ga-NGR-RGD or ^{68}Ga-RGD at 30 min post injection, whereas the tumor uptake of ^{68}Ga-NGR-RGD was much higher than that of ^{68}Ga-RGD at the 1 h time point, indicating longer tumor retention of the heterodimeric tracer ^{68}Ga-NGR-RGD. MCF-7 tumors could not be observed by ^{68}Ga-NGR, which exhibited the lowest uptake among the three tracers. The uptake of ^{68}Ga-NGR-RGD by all organs of interest was higher than that of ^{68}Ga-RGD or ^{68}Ga-NGR, further illustrating that the probe achieved a longer retention time. The significant decrease in the tumor uptake of ^{68}Ga-NGR-RGD after administrating blocking doses of RGD, RGD+NGR, or NGR-RGD demonstrated the specificity of the tracer. It is worth noting that tumors were still visible when blocked with NGR, suggesting that the RGD counterpart was not blocked and contributed to the image. The quantitative biodistribution data were consistent with the findings on the PET/CT images. In summary, dimeric ^{68}Ga-NGR-RGD displayed higher tumor uptake and longer tumor retention compared to monomeric ^{68}Ga-NGR and ^{68}Ga-RGD.

^{68}Ga-NGR-RGD was evaluated and applied in breast cancer xenografts. MCF-7 and MDA-MB-231 tumors could be clearly visualized at 30 min p.i. of ^{68}Ga-NGR-RGD, demonstrating good tumor targeting efficiency in breast cancers expressing either integrin $a_v\beta_3$ or CD13. However, MDA-MB-468 and MX-1 with lower or no expression of $a_v\beta_3$ and CD13 were less visible or invisible. The uptake of ^{68}Ga-NGR-RGD in the MCF-7 tumor was significantly higher than that of MDA-MB-231, MDA-MB-468, and MX-1 at 1 h p.i., showing better affinity of the dimer than of the monomer. Therefore, the dual-targeted peptide-conjugated tracer exhibited the potential to image breast tumors with comparatively lower expression of integrin $a_v\beta_3$ or CD13. Furthermore, ^{68}Ga-NGR-RGD showed good detection ability in the MCF-7 lung metastasis model.

Although the expression level of integrin $a_v\beta_3$ and CD13 of the MCF-7 model selected in our study is relatively low,[24,25] owing to the improved affinity, targeting efficiency, selectivity, and longer retention time of ^{68}Ga-NGR-RGD, the tumor can still be clearly visualized. In fact, the two receptors are highly expressed in many other cancers, such as non-small-cell lung cancer, pancreatic, thyroid, colorectal, and ovarian cancer.[34,35] The two targets were associated with tumor size, lymph node metastasis, tumor differentiation, the metastasis stage, and overall survival in gastric, pancreatic, and colorectal cancer.[30,33,36–38] Therefore, we believe that this dual-target probe can be used more widely, not only for imaging, but also for therapy to cancers and nonmalignant pathologies.

The eventual goal of this project is to develop dual-receptor targeting agents for radiotherapy. Even though ^{68}Ga-NGR-RGD has better targeting efficiency and longer tumor retention, uptake of ^{68}Ga-NGR-RGD in tumors is still relatively low. Therefore, an enhancement of its tumor uptake is highly desirable. One possible solution includes the incorporation of an albumin-binding moiety to prolong the blood circulation time.[39]

5. CONCLUSIONS

In conclusion, we have successfully developed a CD13 and integrin $a_v\beta_3$ dual-receptor targeted tracer, ^{68}Ga-NGR-RGD, for imaging breast cancer. The tracer exhibits high

radiolabeling yield and favorable stability. Preliminary in vitro and in vivo studies demonstrated its excellent tumor targeting efficiency for tumors with these receptors, rendering it as a potential reagent for future clinical translation.

Supplementary Material

Refer to Web version on PubMed Central for supplementary material.

ACKNOWLEDGMENTS

REFERENCES

(1). Goodman SL; Picard M Integrins as therapeutic targets. Trends Pharmacol. Sci 2012, 33, 405–412. [PubMed: 22633092]

(2). Rezazadeh F; Sadeghzadeh N Tumor targeting with ^{99m}Tc radiolabeled peptides: Clinical application and recent development. Chem. Biol. Drug Des 2019, 93, 205–221. [PubMed: 30299570]

(3). Folkman J Angiogenesis in cancer, vascular, rheumatoid and other disease. Nat. Med 1995, 1, 27–30. [PubMed: 7584949]

(4). Chen H; Niu G; Wu H; Chen X Clinical Application of Radiolabeled RGD Peptides for PET Imaging of Integrin $\alpha_v\beta_3$. Theranostics 2016, 6, 78–92. [PubMed: 26722375]

(5). Bhagwat SV; Lahdenranta J; Giordano R; Arap W; Pasqualini R; Shapiro LH CD13/APN is activated by angiogenic signals and is essential for capillary tube formation. Blood 2001, 97, 652–659. [PubMed: 11157481]

(6). Seidi K; Neubauer HA; Moriggl R; Jahanban-Esfahlan R; Javaheri T Tumor target amplification: Implications for nano drug delivery systems. J. Controlled Release 2018, 275, 142–161.

(7). Liu Z; Wang F; Chen X Integrin $\alpha_v\beta_3$-Targeted Cancer Therapy. Drug Dev. Res 2008, 69, 329–339. [PubMed: 20628538]

(8). Hashida H; Takabayashi A; Kanai M; Adachi M; Kondo K; Kohno N; Yamaoka Y; Miyake M Aminopeptidase N is involved in cell motility and angiogenesis: its clinical significance in human colon cancer. Gastroenterology 2002, 122, 376–386. [PubMed: 11832452]

(9). Pierschbacher MD; Ruoslahti E Cell attachment activity of fibronectin can be duplicated by small synthetic fragments of the molecule. Nature 1984, 309, 30–33. [PubMed: 6325925]

(10). Luo H; Hong H; Yang SP; Cai W Design and applications of bispecific heterodimers: molecular imaging and beyond. Mol. Pharmaceutics 2014, 11, 1750–1761.

(11). Yan Y; Chen X Peptide heterodimers for molecular imaging. Amino Acids 2011, 41, 1081–1092. [PubMed: 20232091]

(12). Pilevarzadeh M; Amirshahi M; Afsargharehbagh R; Rafiemanesh H; Hashemi SM; Balouchi A Global prevalence of depression among breast cancer patients: a systematic review and meta-analysis. Breast Cancer Res. Treat 2019, 176, 519–533. [PubMed: 31087199]

(13). Bale R; Putzer D; Schullian P Local Treatment of Breast Cancer Liver Metastasis. Cancers 2019, 11, 1341.

(14). Chaffer CL; Weinberg RA A perspective on cancer cell metastasis. Science 2011, 331, 1559–1564. [PubMed: 21436443]

(15). Medeiros B; Allan AL Molecular Mechanisms of Breast Cancer Metastasis to the Lung: Clinical and Experimental Perspectives. Int. J. Mol. Sci 2019, 20, 2272.

(16). Ranogajec I; Jaki -Razumovi J; Puzovi V; Gabrilovac J Prognostic value of matrix metalloproteinase-2 (MMP-2), matrix metalloproteinase-9 (MMP-9) and aminopeptidase N/CD13 in breast cancer patients. Med. Oncol 2012, 29, 561–569. [PubMed: 21611838]

(17). Rolli M; Fransvea E; Pilch J; Saven A; Felding-Habermann B Activated integrin $a_v\beta_3$ cooperates with metalloproteinase MMP-9 in regulating migration of metastatic breast cancer cells. Proc. Natl. Acad. Sci. U. S. A 2003, 100, 9482–9487. [PubMed: 12874388]

(18). Debordeaux F; Chansel-Debordeaux L; Pinaquy JB; Fernandez P; Schulz J What about $a_v\beta_3$ integrins in molecular imaging in oncology? Nucl. Med. Nucl. Med. Biol 2018, 62-63, 31–46. [PubMed: 29807242]

(19). Máté G; Kertész I; Enyedi KN; Mez G; Angyal J; Vasas N; Kis A; Szabó É; Emri M; Bíró T; Galuska L; Trencsényi G In vivo imaging of Aminopeptidase N (CD13) receptors in experimental renal tumors using the novel radiotracer 68Ga-NOTA-c(NGR). Eur. J. Pharm. Sci 2015, 69, 61–71. [PubMed: 25592229]

(20). Liu Z; Niu G; Wang F; Chen X ^{68}Ga-labeled NOTA-RGD-BBN peptide for dual integrin and GRPR-targeted tumor imaging. Eur. J. Nucl. Med. Mol. Imaging 2009, 36, 1483–1494.

(21). Gai Y; Sun L; Hui W; Ouyang Q; Anderson CJ; Xiang G; Ma X; Zeng D New bifunctional chelator p-SCN-PhPr-NE3TA for copper-64: synthesis, peptidomimetic conjugation, radiolabeling, and evaluation for PET imaging. Inorg. Chem 2016, 55, 6892–6901. [PubMed: 27347690]

(22). Azad BB; Chatterjee S; Lesniak WG; Lisok A; Pullambhatla M; Bhujwalla ZM; Pomper MG; Nimmagadda S A fully human CXCR4 antibody demonstrates diagnostic utility and therapeutic efficacy in solid tumor xenografts. Oncotarget 2016, 7, 12344–12358. [PubMed: 26848769]

(23). Mordant P; Loriot Y; Lahon B; Castier Y; Lesèche G; Soria J-C; Vozenin M-C; Decraene C; Deutsch E Bioluminescent orthotopic mouse models of human localized non-small cell lung cancer: feasibility and identification of circulating tumour cells. PLoS One 2011, 6, No. e26073. [PubMed: 22022511]

(24). von Wallbrunn A; Waldeck J; Höltke C; Zühlsdorf M; Mesters R; Heindel W; Schäfers M; Bremer C In vivo optical imaging of CD13/APN-expression in tumor xenografts. J. Biomed. Opt 2008, 13, No. 011007. [PubMed: 18315356]

(25). Feni L; Parente S; Robert C; Gazzola S; Arosio D; Piarulli U; Neundorf I Kiss and Run: Promoting Effective and Targeted Cellular Uptake of a Drug Delivery Vehicle Composed of an Integrin-Targeting Diketopiperazine Peptidomimetic and a Cell-Penetrating Peptide. Bioconjugate Chem. 2019, 30, 2011–2022.

(26). Zheng Y; Wang H; Tan H; Cui X; Yao S; Zang J; Zhang L; Zhu Z Evaluation of Lung Cancer and Neuroendocrine Neoplasm in a Single Scan by Targeting Both Somatostatin Receptor and Integrin avβ3. Clin. Nucl. Med 2019, 44, 687–694. [PubMed: 31274560]

(27). Murakami H; Yokoyama A; Kondo K; Nakanishi S; Kohno N; Miyake M Circulating aminopeptidase N/CD13 is an independent prognostic factor in patients with non-small cell lung cancer. Clin. Cancer Res 2005, 11, 8674–8679. [PubMed: 16361553]

(28). Zhang S; Zhang Q; Wang J; Zhang H; Zhao D; Zhang Z Expression and clinical significance of aminopeptidase N/CD13 in non-small cell lung cancer. J. Cancer Res. Ther 2015, 11, 223–228. [PubMed: 25879366]

(29). Ikeda N; Nakajima Y; Tokuhara T; Hattori N; Sho M; Kanehiro H; Miyake M Clinical significance of aminopeptidase N/CD13 expression in human pancreatic carcinoma. Clin. Cancer Res 2003, 9, 1503–1508. [PubMed: 12684426]

(30). Cao J; Li J; Sun L; Qin T; Xiao Y; Chen K; Qian W; Duan W; Lei J; Ma J; Ma Q; Han L Hypoxia-driven paracrine osteopontin/integrin avβ3 signaling promotes pancreatic cancer cell epithelial-mesenchymal transition and cancer stem cell-like properties by modulating forkhead box protein M1. Mol. Oncol 2019, 13, 228245.

(31). Kehlen A; Lendeckel U; Dralle H; Langner J; Hoang-Vu C Biological significance of aminopeptidase N/CD13 in thyroid carcinomas. Cancer Res. 2003, 63, 8500–8506. [PubMed: 14679016]

(32). Leith JT; Mousa SA; Hercbergs A; Lin HY; Davis PJ Radioresistance of cancer cells, integrin avβ3 and thyroid hormone. Oncotarget 2018, 9, 37069–37075. [PubMed: 30651936]

(33). Yu S; Li L; Tian W; Nie D; Mu W; Qiu F; Liu Y; Liu X; Wang X; Du Z; Chu WF; Yang B PEP06 polypeptide 30 exerts antitumour effect in colorectal carcinoma via inhibiting epithelial-mesenchymal transition. Br. J. Pharmacol 2018, 175, 3111–3130. [PubMed: 29722931]

(34). Surowiak P; Dr g M; Materna V; Suchocki S; Grzywa R; Spaczyñski M; Dietel M; Oleksyszyn J; Zabel M; Lage H Expression of aminopeptidase N/CD13 in human ovarian cancers. Int. J. Gynecol. Cancer 2006, 16, 1783–1788. [PubMed: 17009972]

(35). Shaw SK; Schreiber CL; Roland FM; Battles PM; Brennan SP; Padanilam SJ; Smith BD High expression of integrin $\alpha v \beta 3$ enables uptake of targeted fluorescent probes into ovarian cancer cells and tumors. Bioorg. Med. Chem 2018, 26, 20852091.

(36). Nohara S; Kato K; Fujiwara D; Sakuragi N; Yanagihara K; Iwanuma Y; Kajiyama Y Aminopeptidase N (APN/CD13) as a target molecule for scirrhous gastric cancer. Clin. Res. Hepatol. Gastroenterol 2016, 40, 494–503. [PubMed: 26774363]

(37). Pang L; Zhang N; Xia Y; Wang D; Wang G; Meng X Serum APN/CD13 as a novel diagnostic and prognostic biomarker of pancreatic cancer. Oncotarget 2016, 7, 77854–77864. [PubMed: 27788483]

(38). Sanz B; Perez I; Beitia M; Errarte P; Fernández A; Blanco L; Estalella I; Loizate A; Irazusta J; López JI; Larrinaga G Aminopeptidase N activity predicts 5-year survival in colorectal cancer patients. J. Investig. Med 2015, 63, 740–746.

(39). Seijsing J; Lindborg M; Höidén-Guthenberg I; Bönisch H; Guneriusson E; Frejd FY; Abrahmsén L; Ekblad C; Löfblom J; Uhlén M; Gräslund T An engineered affibody molecule with pH-dependent binding to FcRn mediates extended circulatory half-life of a fusion protein. Proc. Natl. Acad. Sci. U. S. A 2014, 111, 1711017115.
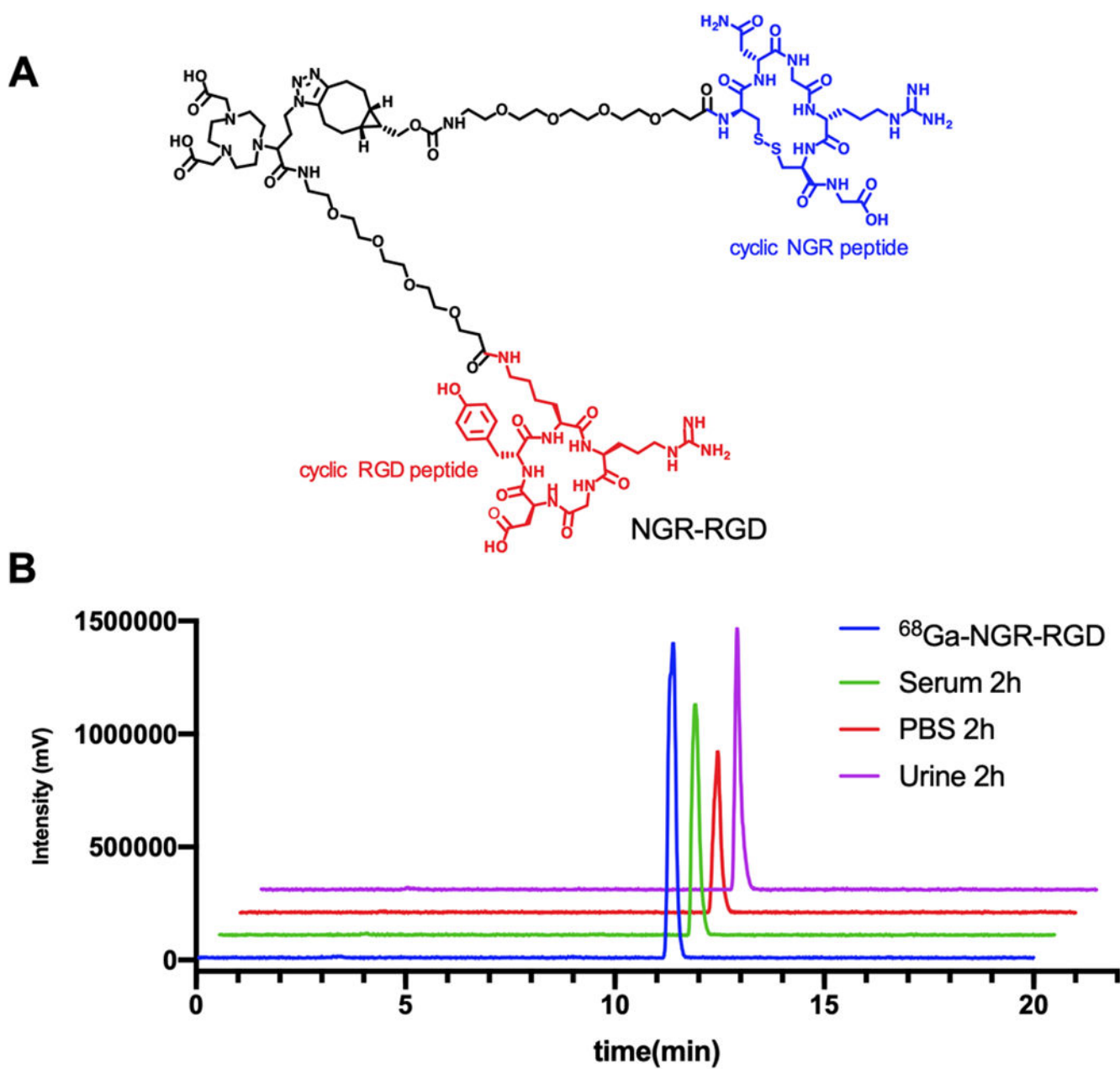
Figure 1.
(A) Chemical structure of NGR-RGD. (B) Analytical radio-HPLC chromatograms of ^{68}Ga-NGR-RGD (blue), 2 h in vitro stability of ^{68}Ga-NGR-RGD in PBS (red) and serum (green), and 2 h in vivo stability of ^{68}Ga-NGR-RGD in urine samples (purple).
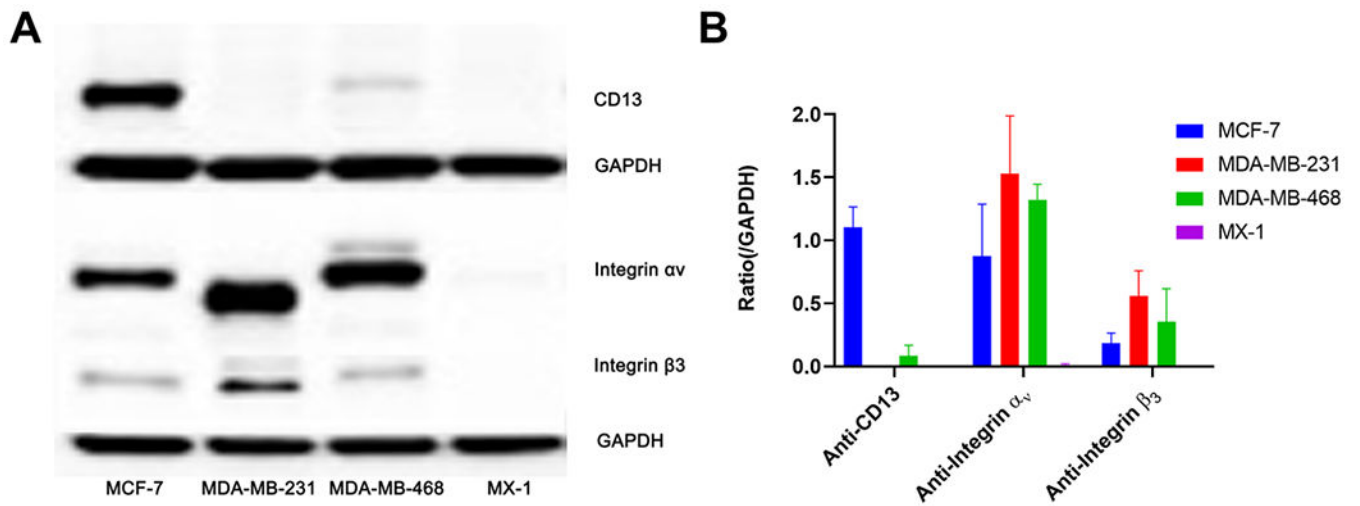
Figure 2.
(A) Western blotting was performed to assess the expression levels of CD13, integrin α_v, and integrin β_3 in MCF-7, MDA-MB-231, MDA-MB-468, and MX-1 cells with GAPDH used as the internal control. (B) The semi-quantitative analysis was conducted through the integrated optical density ratio of CD13, integrin α_v, and integrin β_3 to GADPH (data represent one of three separate experiments, mean ± SD).
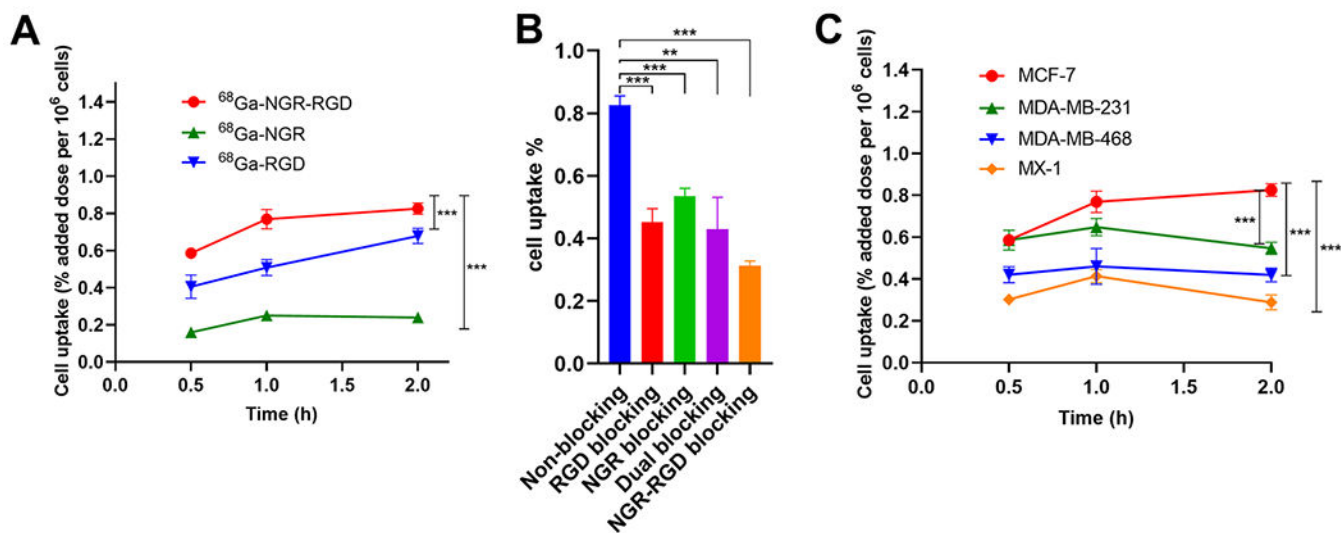
Figure 3.
(A) Uptake of ^{68}Ga-NGR-RGD, ^{68}Ga-NGR, and ^{68}Ga-RGD by MCF-7 cells at 30 min, 1 h, and 2 h. (B) Cell uptake comparison of ^{68}Ga-NGR-RGD with or without blocking doses of RGD, NGR, RGD+NGR, and NGR-RGD in MCF-7 cells. (C) Uptake of ^{68}Ga-NGR-RGD in MCF-7, MDA-MB-231, MDA-MB-468, and MX-1 cells. Three duplicate wells were set in each group. Data are expressed as mean ± SD. (*$P < 0.05$, **$P < 0.01$, ***$P < 0.001$.)
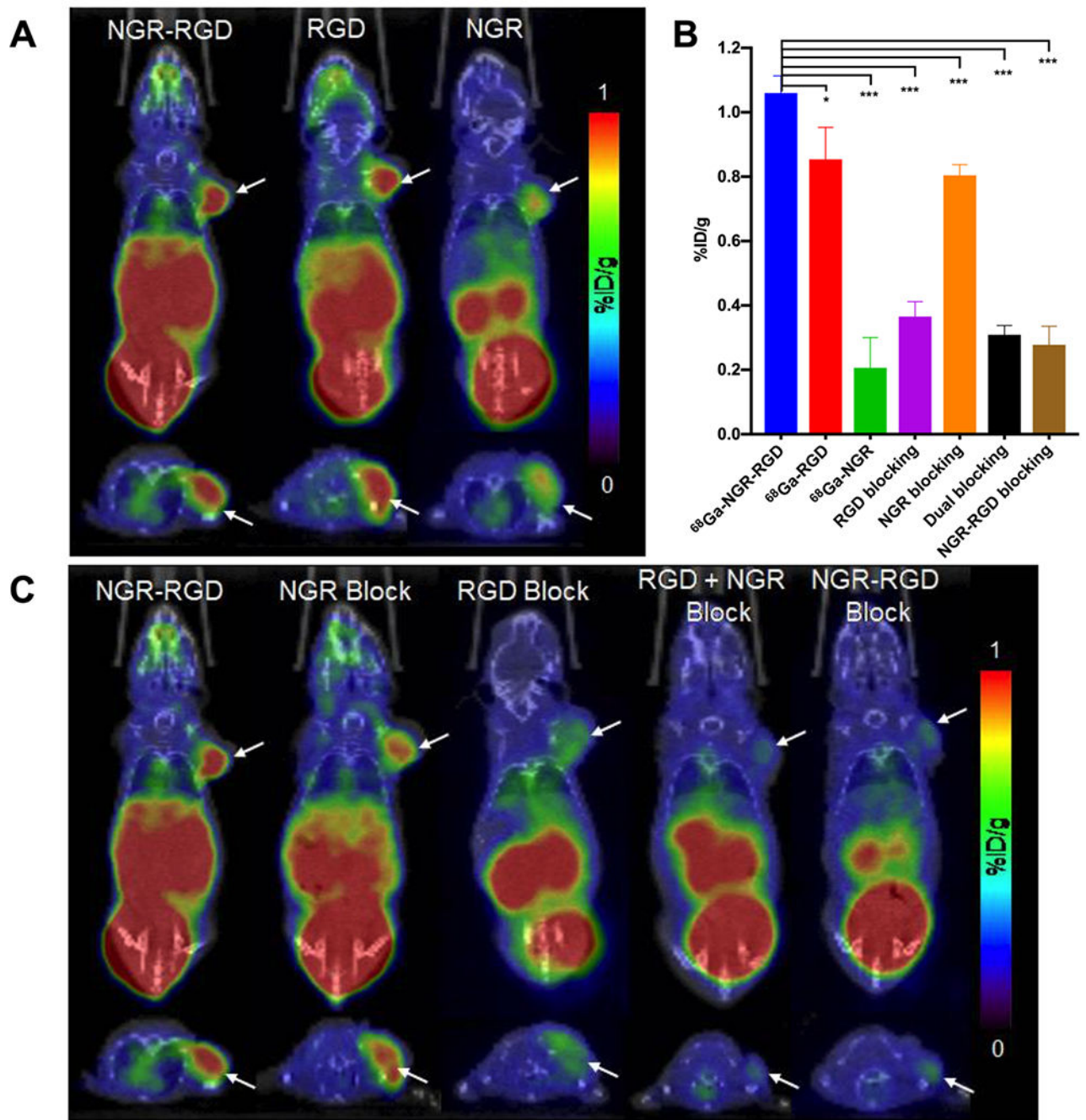
Figure 4.
(A) Representative static PET/CT images of MCF-7 tumor xenograft mice at 30 min p.i. of ^{68}Ga-NGR-RGD, ^{68}Ga-RGD, and ^{68}Ga-NGR (each 6.5–9 MBq). (B) Tumor uptakes determined by quantitative analysis of PET/CT images. (C) Representative static PET/CT images of MCF-7 tumor xenograft mice at 30 min p.i. of ^{68}Ga-NGR-RGD (6.5–9 MBq) with/without blocking agents NGR, RGD, RGD+NGR, or NGR-RGD (20 mg/kg, per mouse). Arrows indicate the location of tumors ($n = 4$ each group). (*$P < 0.05$, **$P < 0.01$, ***$P < 0.001$.)
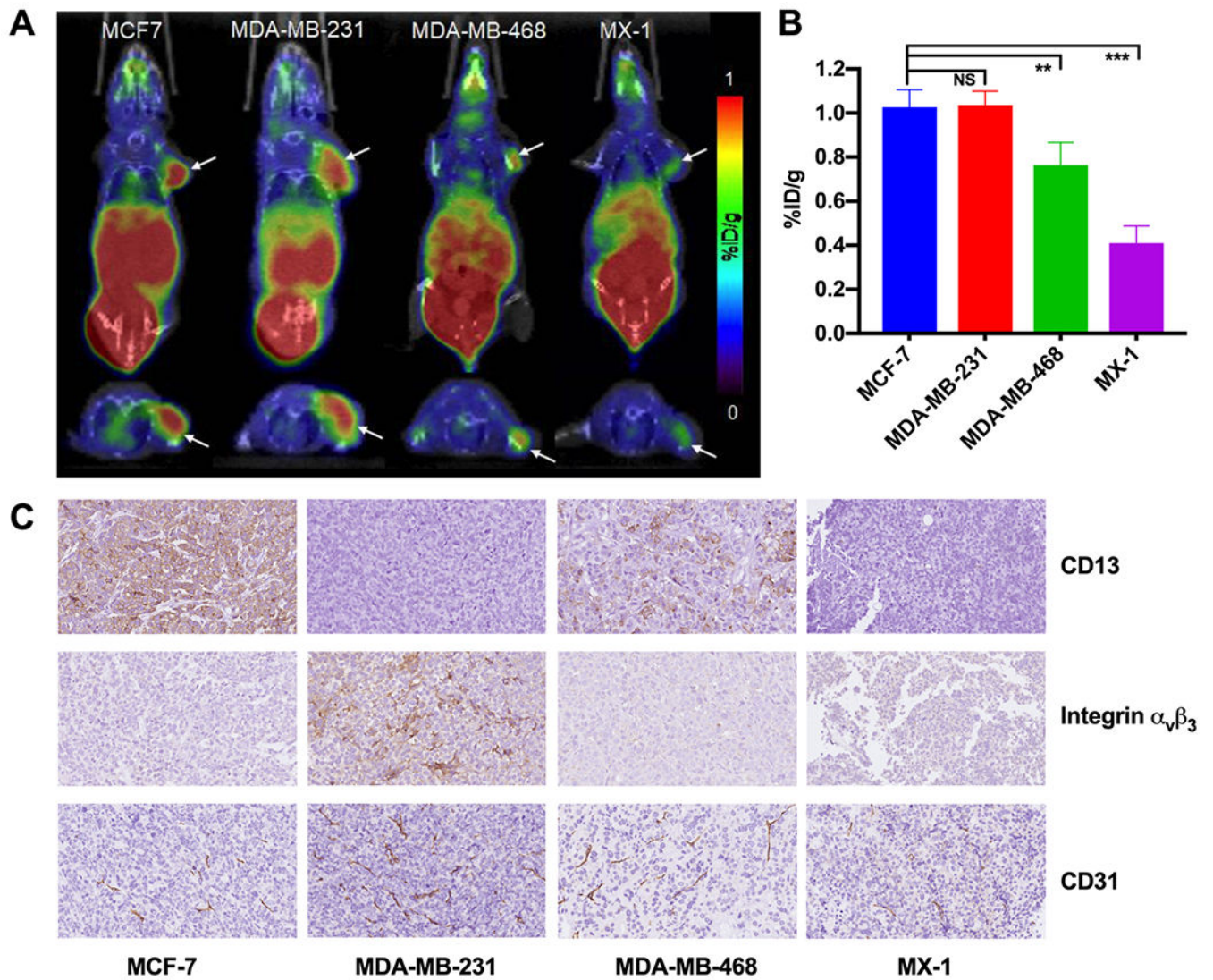
Figure 5.
(A) Representative static PET/CT images of MCF-7, MDA-MB-231, MDA-MB-468, and MX-1 tumor xenograft mice at 30 min p.i. of ^{68}Ga-NGR-RGD (6.5–9 MBq). (B) Tumor uptakes determined by quantitative analysis of PET/CT images. (C) Immunohistochemistry assay of CD13, integrin $\alpha_v\beta_3$, and CD31 in MCF-7, MDA-MB-231, MDA-MB-468, and MX-1 tumors (400 ×). Arrows indicate the location of tumors ($n = 4$ each group).
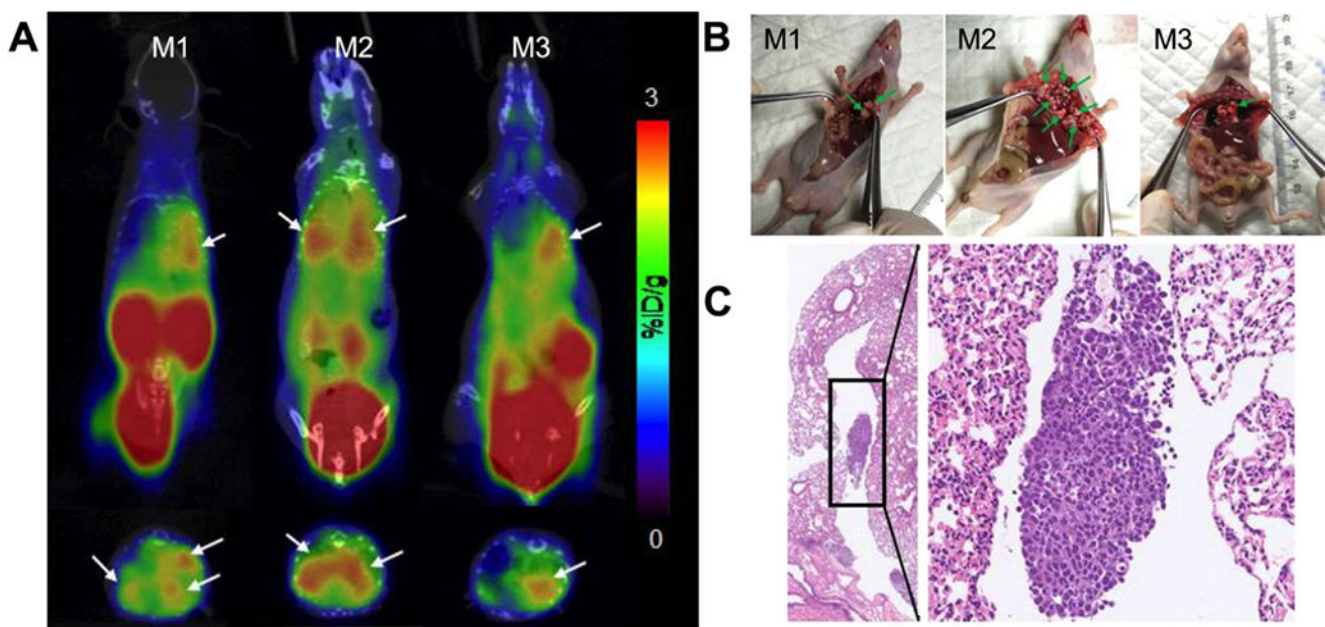
Figure 6.
Small-animal PET/CT imaging and tissue HE changes of MCF-7 pulmonary metastasis mouse models. (A) Representative static PET/CT images of mice with MCF-7 pulmonary metastasis at 1 h p.i. of ^{68}Ga-NGR-RGD (6.5–9 MBq). (B) Diffuse lesions were seen in the left lung. Diffused metastatic lesions were also seen in the right lung of mouse 2. (C) The HE staining confirmed that these lesions were tumor tissues (left 20×; right 200×). Arrows indicate the location of tumors.

Figure 7.
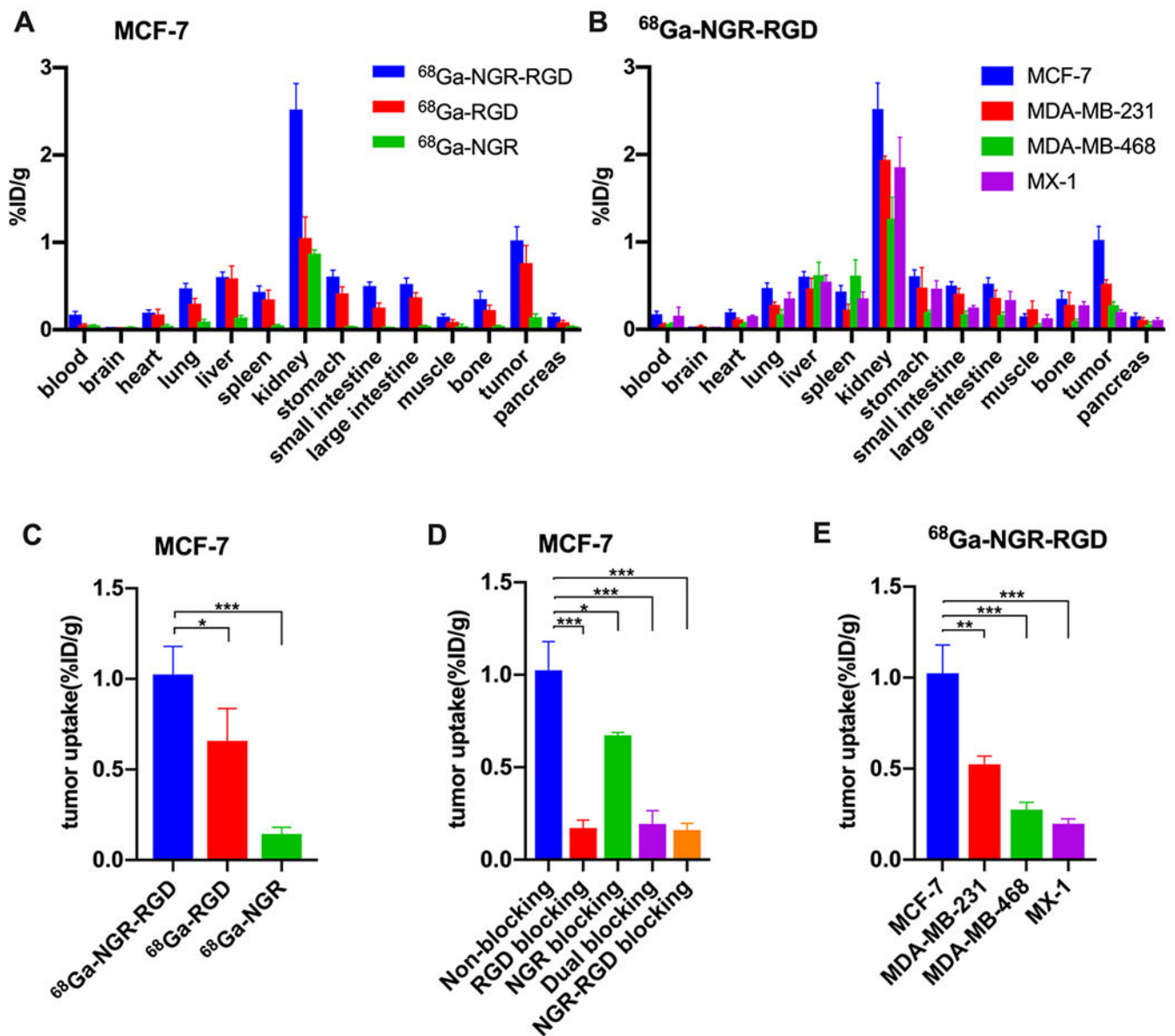Biodistribution studies of ^{68}Ga-NGR-RGD, ^{68}Ga-RGD, and ^{68}Ga-NGR in tumor xenograft mice. (A, C) Biodistribution results and tumor uptake comparisons of ^{68}Ga-NGR-RGD, ^{68}Ga-RGD, and ^{68}Ga-NGR in MCF-7 xenograft mice at 1 h p.i. (D) Tumor uptake comparison of ^{68}Ga-NGR-RGD in MCF-7 tumors with or without coinjection of excess amounts of unlabeled RGD, NGR, RGD+NGR, and NGR-RGD at 1 h p.i. (B, E) Biodistribution results and tumor uptake comparisons of ^{68}Ga-NGR-RGD in MCF-7, MDA-MB-231, MDA-MB-468, and MX-1 xenograft mice. Data are expressed as mean ± SD ($n = 4$ each group). (*$P < 0.05$, **$P < 0.01$, ***$P < 0.001$.)